Combined effects of low temperature and low light intensity on elemental stoichiometry and macromolecules of coccolithophores

Jinlong Shang[1,§], Wenting Ke[2,§], Yinrui Wang[3,§], Junqin Cai[3], Yan Chen[3], Xi Liu[3], Yonghe Han[3], Hong Zhang[3], Kui Xu[4], Yong Zhang[3]

[1]College of Life Science and Xinjiang Key Laboratory of Special Species Conservation and Regulatory Biology, Xinjiang Normal University, Urumqi 830054, Xinjiang, China

[2]School of Primary Education, Wuhan City Polytechnic, Wuhan 430065, China

[3]College of Environmental and Resource Sciences, College of Carbon Neutral Modem Industry, Fujian Key Laboratory of Pollution Control and Resource Recycling, Fujian Normal University, Fuzhou 350117, China

[4]Hubei Key Laboratory of Edible Wild Plants Conservation and Utilization, Hubei Engineering Research Center of Special Wild Vegetables Breeding and Comprehensive Utilization Technology, College of Life Sciences, Hubei Normal University, Huangshi 435002, China

Running head: Temperature and light on coccolithophores

Correspondence to: Wenting Ke (kewenting@whcp.edu.cn); Yong Zhang (yongzhang@fjnu.edu.cn)

[§]These authors contributed equally to this work.

Keywords: coccolithophores, elemental content, low temperature, low light intensity, macromolecules

Abstract

The calcifying coccolithophores *Gephyrocapsa oceanica* and *Emiliania huxleyi* are capable of growing preferentially in deep waters (150–200 m), yet their physiological and biochemical strategies for acclimating to the combined stress of low temperature and low irradiance remain unclear. In this study, we exposed three coccolithophore strains (*G. oceanica* NIES–1318, *E. huxleyi* PML B92/11, and RCC1266) to low temperature (9 ºC) and low light intensity (15 μmol photons m^{-2} s^{-1}), and compared their growth rates, particulate inorganic carbon (PIC), particulate organic carbon (POC), nitrogen (PON) and phosphorus (POP) contents, as well as carbohydrate and lipid levels, with those measured under standard cultivation condition (21ºC, 150 μmol photons m^{-2} s^{-1}). The results showed that low temperature and low light intensity acted synergistically to reduce growth rates, POC contents and the POC : PON and POC : POP ratios, while POP contents remained largely unaffected across all strains. Higher light intensity increased PIC and PON contents under high temperature, but decreased them under low temperature. Low light intensity was identified as the primary driver of reduced carbohydrate and lipid levels. Collectively, these findings suggest that, to acclimate to low–temperature and low–light conditions, coccolithophores prioritized reducing the metabolic cost associated with carbohydrate and lipid biosynthesis, thereby allocating more resources to phosphorus metabolism–a physiological adjustment that could significantly influence biogeochemical cycles in the deep ocean.

1 Introduction

Coccolithophores are unicellular eukaryotic calcifying algae widely distributed throughout the global oceans (Hernández–Almeida et al., 2020). Through photosynthesis, they fix CO_2 into organic carbon, while their calcification process produces $CaCO_3$ (coccoliths) and releases CO_2 into the surrounding environment. This combined effect not only enhances particle settling but also facilitates carbon burial at depth (Skeffington et al., 2022). Hence, coccolithophores are important contributors to the biological and carbonate counter pump (Li et al., 2024). Their comparatively low requirements of nitrogen and phosphorus enable dominance in oligotrophic provinces, e.g., Eastern Mediterranean (Malinverno et al., 2003), and the bloom–forming species such as *Gephyrocapsa oceanica* and *Emiliania huxleyi* can restructure local ecosystem function (Poulton et al., 2014). Notably, coccolithophores are capable of carrying out photosynthesis and osmotrophy (heterotrophic) near or below the base of the euphotic zone (150–200 m)–e.g., in the north–eastern Caribbean and South Pacific Gyre with low temperature (< 12°C) and low irradiance level (< 20 μmol photons m^{-2} s^{-1}), and occupying resource niches that contribute to the stability of deep–water primary production (Jordan and Winter, 2000; Beaufort et al., 2007; Balch et al., 2023). Despite their ecological prominence, the physiological and biochemical strategies that enable coccolithophores to tolerate the combined constraints of low temperature and low irradiance in deeper waters remain poorly resolved.

Prior work has identified several low–temperature acclimate strategies in coccolithophores. Under decreasing temperature, *G. oceanica* increases its cellular particulate organic carbon (POC) and nitrogen (PON) content, while decreases its chlorophyll *a* and alkenone contents (Torres–Romero et al., 2024). The biochemical basis for elevated POC and PON under low temperature may involve a reduction in

enzymatic turnover rates or productivity due to decreased activity of thermally sensitive enzymes, accompanied by an increase in the abundances of these enzymes to partially compensate for their lower efficiency (Petrou et al., 2016). For instance, the abundance of the carboxylating enzyme Rubisco (Ribulose–1,5–bisphosphate carboxylase/oxygenase) is two to three times higher in phytoplankton from the Southern Ocean than in those from temperate oceans (Sage, 2002; Young et al., 2015). Additionally, the coccolithophore *G. oceanica* and *E. huxleyi* produce unsaturated long–chain alkenones (C37–C39) (Conte et al., 1998) and increase their degree of unsaturation to modulate the microstructure of membrane lipids, thereby enhancing membrane stability under low temperature conditions (Conte et al., 2006). Together, these studies elucidate the physiological and biochemical mechanisms underlying coccolithophore adaptation to low temperatures (Dedman et al., 2023; Torres–Romero et al., 2024). However, little attention has been paid to the biogeochemical consequences of coccolithophores under low temperature conditions, particularly the responses of their carbon (C) : nitrogen (N) : phosphorus (P) ratios and the potential impacts on deep–sea ecosystems.

Coccolithophores exhibit unique features in their response to low light conditions. Recently, Shen et al. (2025a) purified a photosystem I (PSI)–fucoxanthin chlorophyll a/c–binding protein (PSI–FCPI) supercomplex from the coccolithophore *E. huxleyi* (Eh). This monomeric supercomplex contains 12 PSI core subunits, a specific lumenal linker protein (EhLP), and 38 peripheral Eh–FCPI antennae, making it the largest PS–antenna supercomplex known to date. The high levels of chlorophyll c and fucoxanthin in this supercomplex enable fast kinetics and efficient absorption of blue–green light, which is particularly suited to the deep–ocean environment where *E. huxleyi* dwells (Shen et al., 2025a). Under low light intensity, coccolithophore increases their

functional absorption cross–section, quantum efficiency, and contents of Chl *a* and carotenoid to enhance light absorption (Zhang and Gao, 2021). Moreover, the refractive index of coccoliths (approximately 1.65) is higher than that of seawater (approximately 1.33) (Horváth and Varjú, 2004). This structure feature allows coccoliths to acts as micro–lenses, focusing incoming blue–green light onto the chloroplasts and thereby increasing local light intensity (Young et al., 1999). Such light–concentrating effect can enhance photosynthetic efficiency, especially in the deep ocean (Triccas et al., 2025). However, to our knowledge, few studies have examined the variation in physiological and biochemical characteristics among different coccolithophore strains in response to low light intensity.

Most research on the combined effects of temperature and light intensity on coccolithophores has focused on range of 10–24ºC and 60–480 μmol photons m^{-2} s^{-1} (Feng et al., 2008; Jin et al., 2019; Zhang et al., 2020), leaving the extreme condition of simultaneous low temperature and low light intensity largely unexplored. In this study, we exposed three coccolithophore strains to low temperature (9ºC) and low light (15 μmol photons m^{-2} s^{-1}), and compared their growth rates, particulate organic carbon (POC), nitrogen (PON) and phosphorus (POP), carbohydrate and lipid contents with those measured under standard cultivation conditions (21ºC and 150 μmol photons m^{-2} s^{-1}). The aim was to investigate the physiological and biochemical responses of coccolithophores to these combined stressors and to assess their potential implications for the deep–sea carbon cycle.

2 Materials and methods

2.1 Strains and culture conditions

Gephyrocapsa oceanica strain NIES–1318 was originally isolated from the coastal

126 water in the East China Sea, and obtained from the center for collections of marine
127 bacteria and algae, Xiamen University, China. *Emiliania huxleyi* strain PML B92/11
128 was isolated from the coastal waters off Bergen, Norway (60 ºN, 5 ºE), and obtained
129 from the plymouth algal culture collection, UK. *Emiliania huxleyi* strain RCC1266 was
130 isolated from shelf waters around Ireland (49º30'N, 10º30'W), and obtained from the
131 roscoff algal culture collection, France (Jin et al., 2019; Zhang et al., 2021).
132 In the control treatment, cells were maintained in 150 μmol photons m^{-2} s^{-1} of
133 photosynthetically active radiation (PAR, high light intensity, HL) (measured using a
134 PAR Detector, PMA 2132 from solar light company) under a 16 h: 8 h light : dark cycle
135 (light period: 06:00 to 22:00 h) at 21.0 ºC (high temperature, HT) in semicontinous
136 cultures. To simulate deep–sea temperature and light intensity, experimental treatments
137 included low temperature (LT: 9.0 ºC), low light intensity (LL: 15 μmol photons m^{-2} s^{-}
138 ^{1}) and combination of low temperature and low light intensity (LTLL: 9.0 ºC and 15
139 μmol photons m^{-2} s^{-1}) (Jordan and Winter, 2000; Beaufort et al., 2007). Therefore, there
140 were four treatments in this study: (1) 9.0 ºC and 15 μmol photons m^{-2} s^{-1} (LTLL), (2)
141 9.0 ºC and 150 μmol photons m^{-2} s^{-1} (LTHL), (3) 21.0 ºC and 15 μmol photons m^{-2} s^{-1}
142 (HTLL), (4) 21.0 ºC and 150 μmol photons m^{-2} s^{-1} (HTHL, control), and three replicates
143 for each treatment.
144 Three strains were cultured in natural seawater obtained from the Pingtan Island,
145 Southeast China. The seawater was first filtered using a membrane filter (0.45 μm pore
146 size, CN-CA, Chuangwei), sterilized at 121ºC for 20 minutes, and enriched with 64
147 μmol L^{-1} NO^{3-}, 4 μmol L^{-1} PO_4^{3-}, f/8 concentrations for trace metal and vitamin
148 solutions (Guillard and Ryther 1962). Then enriched seawater was aerated with sterile
149 ambient air (PVDF 0.22 μm pore size, Simplepure, Haining) with about 400 μatm
150 partial pressure of CO_2 for 24 hours, and sterilized by gentle pressure filtration (0.22

μm pore size, Polycap 75 AS, Whatman) and carefully pumped into autoclaved 500 mL and 2000 mL polycarbonate (PC) bottles.

Three strains were cultured at 21.0 ºC and 150 μmol photons m^{-2} s^{-1} with an initial cell concentration of about 3000 cells mL^{-1} and cultures were diluted every 3 days and maintained in exponential growth for 9 days with a minimum of 10 generations. After that, the cells of the same initial concentrations as above were transferred from 21.0 ºC and 150 μmol photons m^{-2} s^{-1} (HTHL) to 21.0 ºC and 15 μmol photons m^{-2} s^{-1} (HTLL) and to 9.0 ºC and 150 μmol photons m^{-2} s^{-1} (LTHL), and then from 9.0 ºC and 150 μmol photons m^{-2} s^{-1} to 9.0 ºC and 15 μmol photons m^{-2} s^{-1} (LTLL). Cultures were diluted every 3 or 4 days, and maintained in exponential growth for 15 or 16 days under the HTLL and LTHL treatments, and for 32 days for *G. oceanica* strain and for 20 days for two *E. huxleyi* strains under the LTLL treatment, which were dependent on cell division rates per day of each strain (Figure S1). Culture bottles were mixed three times per day at 09:00 h, 14:00 h and 18:00 h. In the last day of the incubation under each treatment, subsamples were taken for measurements of cellular contents of the total particulate carbon (TPC), particulate organic carbon (POC), nitrogen (PON) and phosphorus (POP), carbohydrate, lipid and chlorophyll (Chl) *a*.

2.2 Cell density measurement

After mixing, 2 mL samples for cell concentration measurement were taken daily at 14:00 h, and fixed with 10 μL Lugol's solution (a mixture of potassium iodide, iodine and sodium acetate). Then 1 mL samples were added into the counting chamber (Sedgwich–Rafter, S52, Graticules), and cell concentration was quantified by cell counting using a biological microscope (E100, Nikon Eclipse). Growth rate (μ) was calculated according to the equation: $\mu = (\ln N_1 - \ln N_0) / d$, where N_0 and N_1 were cell

concentrations at the beginning and the end of a growth interval, and *d* was the duration of the growth period in days (Wang et al., 2024).

2.3 Element content measurements

Samples for determinations of TPC (300 mL), POC and PON (300 mL), and POP (300 mL) contents were gently filtered onto GF/F filters (pre–combusted at 450 ºC for 5 hours) at 15:00 hour under each treatment. TPC, POC and POP samples were stored in the dark at –20 ºC. For POC measurements, samples were fumed with HCl for 12 hours to remove inorganic carbon. Then POC and TPC samples were dried at 60 ºC for 12 hours and analyzed using an Elemental CHNS analyser (Vario EL cube, GmbH, Germany). Cellular particulate inorganic carbon (PIC) content was calculated as the difference between TPC and POC (Fabry and Balch, 2010). To remove dissolved inorganic phosphorus from the GF/F filters, POP samples were rinsed three times with 5 mL 0.17 mol L^{-1} Na_2SO_4. After that, 2 mL 0.017 mol L^{-1} $MgSO_4$ solution was added onto filters. Then POP samples were dried at 90 ºC for 12 hours and combusted at 500 ºC for 6 hours to remove POC, then cooled and extracted by hydrolysis with 0.2 mol L^{-1} HCl (Solórzano and Sharp, 1980). Phosphorus concentrations were determined using the ammonium molybdate method using adenosine–5–triphosphate disodium trihydrate (ATP007, Bioshop) as a standard.

2.4 Chlorophyll *a*, carbohydrate and lipid analyses

After mixing, samples for analyses of chlorophyll (Chl) *a* (100 mL), carbohydrate (500 mL) and lipid (300 mL) were obtained by filtering onto pre–combusted GF/F filters (at 450 ºC for 5 hours) at 15:00 hour under each treatment. Five milliliters of 90% acetone was used to extract the Chl *a* at 4 ºC for 24 hours. Then samples were centrifuged at

8000 rpm for 10 min at 4 °C and the absorbances of the supernatant were determined between 600–800 nm using a UV spectrophotometer (P5, Shanghai Mepada Instruments Ltd., China). Chl *a* concentration (μg L^{-1}) of sample was calculated as follows (Ritchie 2006).

$$\text{Chl } a = 11.93 \times (A_{664} - A_{750}) - 1.93 \times (A_{647} - A_{750})$$

where A_{647}, A_{664} and A_{750} were the absorbance values of supernatant at 647, 664 and 750 nm.

Carbohydrate samples were pretreated with 12.00 mol L^{-1} of sulfuric acid (H_2SO_4) in the dark for 1 hour, and then diluted by Milli–Q water to a final H_2SO_4 concentration of 1.20 mol L^{-1}. Then samples were sonicated for 5 min, vortexed for 30 s and boiled at 90.0 °C for 3 hours (Pakulski and Benner, 1992). The concentration of monosaccharide was determined at 490 nm by phenol–sulfuric reaction with glucose as standard (Masuko et al., 2005).

Lipid samples were extracted with 2 mL dimethyl sulfoxide–methanol (v : v = 1 : 9), sonicated for 15 min, boiled at 60 °C for 30 min. Then samples were centrifuged (5 min, 6000×g), and the oil–containing supernatants were transferred to a new tube (A, wight W_A) (Xu et al., 2020). The residue samples were treated with 4 mL ether–n–hexane (v : v = 1 : 1) for 1.5 h at 4 °C. Then samples were centrifuged again and the supernatants were transferred to tube A again. The lipid–containing phase was dried using a nitrogen blower and then tube A was weighed (wight W_B) again. The lipid content was calculated as the difference between W_B and W_A.

2.5 Data Analysis

A two–way analysis of variance (ANOVA) was used to determine the main effect of temperature and light intensity and their interactions for all variables in this study. A

Tukey post hoc test was performed to identify significant differences between two levels of each treatment. A Shapiro–Wilk test was conducted to analyze the normality of residuals, and a Levene test was conducted to test for homogeneity of variances. The significant difference between treatments was set as $p \leq 0.05$. Data analysis and visualizations were made using R v.3.6.1 (R Core Team 2018) and packages ggplot2 v.3.2.0.

3 Results

3.1 Growth rate and cellular Chl *a* content

Low temperature and low light intensity acted synergistically to decrease growth rates of three strains, which can be seen by comparing growth rates in high temperature and high light (HTHL) condition with those in high temperature and low light (HTLL), low temperature and high light (LTHL), and low temperature and low light (LTLL) conditions (Tables 1, 2; Figure 1a, b, c). Compared to HTHL, growth rates of *G. oceanica* NIES–1318 decreased by 34% ± 3% in HTLL, by 48% ± 1% in LTHL, and by 81% ± 3% in LTLL (Tukey, all $p < 0.01$) (Figure 1a). Similarly, compared to HTHL, growth rates of *E. huxleyi* PML B92/11 decreased by 38% ± 1% in HTLL, by 52% ± 1% in LTHL, and by 63% ± 3% in LTLL (Tukey, all $p < 0.01$) (Figure 1b). As to *E. huxleyi* RCC1266, compared to HTHL, growth rates decreased by 33% ± 3% in HTLL, by 48% ± 2% in LTHL, and by 64% ± 3% in LTLL (Tukey, all $p < 0.01$) (Figure 1c).

The effect of light intensity on cellular Chl *a* content depends on temperature. At high temperature (HT), decreasing light (LL) intensity increased the Chl *a* content of *E. huxleyi* PML B92/11 by 45% ± 11% (Tukey, $p < 0.01$) (Figure 1e), and did not

significantly affect the Chl *a* contents of *G. oceanica* NIES–1318 and *E. huxleyi* RCC1266 (Figure 1d, f). At low temperature (LT), decreasing light intensity did not significantly increase the Chl *a* of three strains (Tukey, all $p > 0.2$) (Figure 1d, e, f).

3.2 Cellular PIC, POC, PON and POP contents

The effect of light intensity on cellular PIC, POC and PON contents depends on temperature, which can be seen by comparing these parameters in the high temperature (HT) regimes with their paired low temperature (LT) regimes (Tables 1, 2; Figure 2). At HT, compared to HL intensity, low light (LL) intensity decreased the PIC contents by 38% ± 5% for *G. oceanica* NIES–1318 (Tukey, $p < 0.01$) (Figure 2a), by 29% ± 19% for *E. huxleyi* PML B92/11 (Tukey, $p = 0.11$) (Figure 2b), by 23% ± 7% for *E. huxleyi* RCC1266 (Tukey, $p = 0.04$) (Figure 2c). However, at LT, decreasing light intensity increased the PIC contents by 60% ± 11% for *G. oceanica* NIES–1318 (Tukey, $p < 0.01$) (Figure 2a), by 109% ± 32% for *E. huxleyi* RCC1266 (Tukey, $p = 0.04$) (Figure 2c).

At HT, compared to HL intensity, low light (LL) intensity decreased the POC contents by 29% ± 4% for *G. oceanica* NIES–1318, by 39% ± 7% for *E. huxleyi* PML B92/11, and by 32% ± 6% for *E. huxleyi* RCC1266 (all $p < 0.01$) (Figure 2d,e,f). The response of PON contents to low temperature and low light conditions was similar to that of PIC contents. At HT, compared to HL intensity, LL intensity decreased the PON contents by 9% ± 10% for *G. oceanica* NIES–1318 ($p > 0.50$) (Figure 2g), by 19% ± 4% for *E. huxleyi* PML B92/11 ($p < 0.01$) (Figure 2h), and by 19% ± 2% for *E. huxleyi* RCC1266 ($p = 0.21$) (Figure 2i). However, at LT, decreasing light intensity increased the PON contents by 31% ± 16% for *G. oceanica* NIES–1318 ($p = 0.12$)

(Figure 2g), by 29% ± 11% for *E. huxleyi* PML B92/11 ($p = 0.03$) (Figure 2h), and by 50% ± 32% for *E. huxleyi* RCC1266 ($p = 0.12$) (Figure 2i). Interestingly, compared to HTLL, low temperature and low light intensity did not significantly affect the POP contents of three strains (all $p > 0.05$) (Figure 2j,k,l).

3.3 PIC : POC, POC : PON, POC: POP and PON : POP ratios

The effects of temperature and light intensity on the PIC : POC ratio are strain–specific (Table 1; Figure 3). As to *G. oceanica* NIES–1318, compared to HTHL, PIC : POC ratio didn't be affected significantly in HTLL and LTHL, whereas increased by 63% ± 13% in LTLL ($p < 0.01$) (Figure 3a). As to *E. huxleyi* PML B92/11, decreasing temperature and light intensity did not significantly affect the PIC : POC ratio (Figure 3b) (all $p > 0.20$). As to *E. huxleyi* RCC1266, compared to HTHL, PIC : POC ratio decreased by 63% ± 6% in LTHL ($p < 0.01$) (Figure 3c).

Low temperature and low light intensity acted synergistically to decrease the POC : PON ratios and POC : POP ratios of three strains, which can be seen by comparing these parameters under the HTHL treatment with HTLL, LTHL and LTLL treatments (Figure 3d–i). Compared to HTHL, POC : PON ratio of *G. oceanica* NIES–1318 decreased by 21% ± 9% in HTLL ($p = 0.07$), by 35% ± 5% in LTHL ($p < 0.01$), and by 56% ± 6% in LTLL ($p < 0.01$) (Figure 3d). As to *E. huxleyi* PML B92/11, compared to HTHL, POC : PON ratio decreased by 20%–46% in HTLL, LTHL, and LTLL (all $p < 0.05$) (Figure 3e). As to *E. huxleyi* RCC1266, compared to HTHL, POC : PON ratio decreased by 15%–52% in HTLL ($p = 0.13$), LTHL ($p = 0.18$) and LTLL ($p < 0.01$) (Figure 3f). At HT, decreasing light intensity decreased the POC : POP ratios by 24%–33% for three strains (all $p < 0.06$) (Figure 3g,h,i). At LT, decreasing light intensity did

not significantly affect the POC : POP ratios of three strains (Figure 3g, h, i). Compared to HL intensity, at HT, low light (LL) intensity did not significantly decrease the PON : POP ratios of three strains, whereas at LT, it increased the PON : POP ratios by 53%–57% (Figure 3j,k,l) (both $p < 0.05$ for *G. oceanica* NIES–1318 and *E. huxleyi* PML B92/11; $p = 0.08$ for *E. huxleyi* RCC1266).

3.4 Cellular carbohydrate and lipid contents

Cellular carbohydrate and lipid contents were mainly affected by light intensity, which can be seen by comparing these parameters in the HL intensity with their paired LL intensity (Table 1; Figure 4). Compared to HL intensity, in LL intensity, the carbohydrate contents were significantly lower for three strains regardless of levels of temperature for the range used here (Figure 4a,b,c). Compared to HL intensity, at HT, low light intensity decreased the carbohydrate contents by 80%–83% for three strains (all $p < 0.01$), and at LT, it decreased the carbohydrate contents by 85%–88% (all $p < 0.01$) (Figure 4a,b,c). Similarly, compared to HL intensity, at HT, low light intensity decreased the lipid contents by 63%–69% of three strains (all $p < 0.01$), and at LT, it decreased the lipid contents by 76%–85% (all $p < 0.01$) (Figure 4d,e,f).

4 Discussion

We propose that under low temperature and low light intensity (LTLL), coccolithophores slow their metabolism, resulting in reduced growth rates and lower levels of POC, POP, carbohydrates and lipids. Our results reveal a distinct acclimation strategy: energy conservation is prioritized through an initial reduction in carbohydrate and lipid content, followed by a subsequent decrease in growth rate (Figure 4). Notably, carbohydrate and lipid levels were primarily light–dependent, whereas PON (a proxy

for protein) was temperature–dependent. Analysis of the POC : PON : POP ratios showed that POC decreased more steeply than PON, only under high temperature did POC decline more steeply than POP (Figure 3). Intriguingly, under low temperature, both POC and POP were insensitive to light, whereas high light intensity inhibited PON. Collectively, these results indicate that coccolithophores acclimate to LTLL conditions by precisely regulating their biomolecular composition, elemental stoichiometry and growth (Zhang et al., 2021).

Effects of low temperature and light limitation on the elemental stoichiometry and macromolecules of coccolithophores

While previous studies observed stable or even increased POC contents at moderate temperature decreases (e.g., from 18–24 ºC down to 14–20 ºC) (Feng et al., 2008; Borchard et al., 2011; Tong et al., 2019; Torres–Romero et al., 2024), our results demonstrate a significant decline in POC at 9 ºC compared to 21 ºC (Figure 2). This discrepancy likely stems from the several inhibitory effect of 9 ºC on photosynthetic carbon fixation and growth rates, which is far more pronounced than the effects seen at 14 ºC or 15 ºC (Shen et al., 2025b). The stability of POC contents across both light intensities at 9 ºC further supports this threshold effect. Additionally, the broad temperature and light gradients employed in this study may have overshadowed any subtle inter–strain variations in POC.

Compared to the LTLL condition, the combination of low temperature and high light (LTHL) led to a threefold increase in carbohydrate and lipid contents, even as total POC remained relatively stable. This stoichiometric shift implies a reduction in protein content, a conclusion corroborated by the decline in PON (Figures 2, 4). The reasons could be that at 9 ºC, cellular metabolism is significantly constrained, rendering a PAR

of 150 μmol photons m^{-2} s^{-1} excessive rather than productive (Jin et al., 2019). Consequently, the cell reallocates surplus energy into carbohydrates and lipids as a photoprotective mechanism. This is supported by the significantly lower carbohydrate : POC and lipid : POC ratios under low light (Figure S2), whereas the higher ratios observed at low temperature under high light reflect a strategy favoring energy storage (Zhang et al., 2021). Furthermore, while POC and PON typically exhibit an optimal irradiance response (Zhang et al., 2015), our data show that high light reduces PON content at low temperature (Figure 2). This suggests that low temperature depresses the optimal light threshold for protein synthesis and diminishes high light tolerance (Gafar et al., 2018). The suppressed Calvin cycle at 9 °C limits carbon fixation, reducing energy demand and necessitating the downregulation of Chl *a* (Figure 1). Notably, under high light, cells further downregulate light–harvesting antenna proteins to prevent the absorption of detrimental excess light, a process that significantly contributes to the observed decrease in PON (McKew et al., 2013).

Interestingly, the combination of low temperature and low light did not significantly alter the POP content of coccolithophores (Figure 2j–l). This stability may be attributed to a synchronized metabolic slowdown: while low light limits photosynthetic efficiency, low temperature suppresses respiratory, leading to a concurrent reduction in both adenosine triphosphate (ATP) synthesis and overall energy consumption (Jin et al., 2019; Strzepek et al., 2019). This coordination maintains a dynamic equilibrium between phosphorus consumption (e.g. for ATP synthesis) and supply (e.g. phosphorus uptake) (Dyhrman, 2016). Furthermore, as energy–intensive processes like carbohydrate or lipid synthesis and cell division are inhibited (Figures 4, 1), coccolithophores prioritize phosphorus allocation toward essential biomolecules. Specifically, phosphorus is channeled into nucleic acids (DNA or RNA) and membrane

phospholipids at the expense of non–essential metabolic pathways (Zhang et al., 2021). Notably, low temperature–rather than light–appears to be the primary driver for increased RNA investment, a strategy that preserves core POP pools despite a sluggish metabolism (Zhang et al., 2021). From an ecological perspective, the resilience of POP under these stressors may enhance the competitive fitness of coccolithophores in high–latitude or deep–euphotic environments (Perrin et al., 2016). Given that phosphorus often limits deep–sea phytoplankton, stable cellular POP levels could influence zooplankton grazing efficiency, thereby modulating energy transfer and nutrient cycling within deep–sea ecosystems (Gerecht et al., 2014).

Effects of low temperature and light limitation on calcification and growth rate of coccolithophores

While calcification is typically energy–dependent and stimulated by high light under temperate conditions (Triccas et al., 2025), we observed a counterintuitive reduction in PIC content under high light during cold stress (Figure 2a–c). This finding challenges the conversional view that calcification is primarily limited by energy availability under low light (Zhang et al., 2015). We propose that low temperature (LT) reduces the repair capacity of photosynthetic machinery, making cells more susceptible to photoinhibition. This, in turn, likely damages cellular membranes and disrupts the ion transport (e. g., Ca^{2+} or HCO_3^-) and homeostasis essential for calcification (Strzepek et al., 2019; Triccas et al., 2025). Furthermore, the observed restriction of ribosomal proteins and the potential downregulated of calcium–binding proteins–despite an abundance of photosynthetic machinery at low temperatures–may further depress PIC accumulation (Dedman et al., 2023). From an ecological standpoint, high PIC content serves as a defense against grazers, while an elevated PIC : POC ratio enhances carbon

sedimentation and sequestration in the deep sea (Poulton et al., 2014; Rigual–Hernández et al., 2020). Notably, the significant strain–specific variation in PIC content observed here, highlights the phenotypic plasticity that allows coccolithophores to colonize diverse marine habitats, ranging from sunlit surfaces to the deep euphotic zone (Rigual–Hernández et al., 2018).

Previous studies reported growth rates of *E. huxleyi* ranging from 0.09 d^{-1} (strain CCMP371 at 8.5 ºC) to 0.12–0.19 d^{-1} (strains RCC1710, RCC1252, and RCC1710 at 6.5 ºC) (Rosas–Navarro et al., 2016; Wang et al., 2019). Additionally, PIC contents of *E. huxleyi* strain CCMP371 were observed at 3.2–4.8 pg $cell^{-1}$ at 8.5 ºC (Wang et al., 2019). Synthesizing these findings with our results, we estimate that the growth rates of the three coccolithophore strains in this study would be approximately 0.1 d^{-1} at 4 ºC, with PIC contents around 3–4 pg $cell^{-1}$. Notably, the lower latitudinal origin of *G. oceanica* compared to strains RCC1266 and PML B92/11 suggests a superior adaptation to warmer waters (Buitenhuis et al., 2008). Consequently, *G. oceanica* exhibits a more pronounced decline in growth rate under cold stress, driving the observed strain–specific divergence. Furthermore, rising temperatures stimulate PIC accumulation more effectively in *E. huxleyi* than in *G. oceanica*. As a result, thermal warming leads to a decreased PIC : POC ratio in *G. oceanica*, whereas the ratio remains relatively stable in *E. huxleyi*.

Under laboratory conditions (9 ºC and 15 μmol photons m^{-2} s^{-1}), the three coccolithophore strains maintained growth rates of 0.24 to 0.46 d^{-1}, equivalent to a division cycle of approximately 2–3 days. In contrast, within the actual ocean at depths of 100–200 m, cells may cease division entirely, opting instead to expand light–harvesting antenna protein or the functional cross–sectional area of PSII reaction centers to ensure survival (Pierangelini et al., 2015). This strategy preserves their

capacity for rapid recovery and reproduction once favorable conditions return. While our experimental POC, PON, POP and PIC values align closely with the global averages synthesized by Sheward et al. (2023), the physiological characteristics of phytoplankton in situ are further reshaped by complex environmental drivers. Because other environmental factors, such as hydrostatic pressure, nutrient pulses, microbial interactions, and spectral light quality, can affect these physiological characteristics of phytoplankton. In the dysphotic zone, high hydrostatic pressure may inhibit tubulin polymerization and membrane fluidity, thereby suppressing photosynthesis and cell division (Potts and Friedmann, 1981). Conversely, nutrient pulses provide the essential substrates for synthesizing key proteins even under depressed metabolic rates (Sui et al., 2019), while microbial interactions dictate the balance between survival or decomposition (Zweifel et al., 2025). Furthermore, spectral light quality–specifically the dominance of blue light at 100–150 m–acts as a critical signal. Coccolithophores adapt to this "blue light regime" by enriching their antennae with chlorophyll c and fucoxanthin to maximize absorption efficiency (Shen et al., 2025b). Most notably, recent findings by Balch et al. (2023) indicate that at depths where light is as low as 2 μmol photons m^{-2} s^{-1}, coccolithophores can utilize osmotrophy–the uptake of dissolved organic carbon (DOC) such as acetate, mannitol and glycerol–to sustain both POC and PIC production. Although DOC–supported growth rates remain low, this osmotrophic capability serves as a vital survival strategy under extreme light limitation. Such mixotrophic behavior underscores that coccolithophore–mediated DOC uptake is a significant yet underappreciated component of the biological carbon pump (Balch et al., 2023). Ultimately, the intricate interplay among these physical, chemical, and biological factors redefines the ecological functions of coccolithophores in the deep ocean. In addition, the nutrient concentrations in this study exceed typical levels found

448 in the open ocean's surface or subsurface waters. These nutrient–replete conditions
449 were intentionally maintained to decouple the physiological effects of temperature and
450 light from nutrient stress. Consequently, when extrapolating our findings to natural
451 environments, one must account for the potential of nutrient limitation to modulate or
452 attenuate the observed responses.
453
454 **Implications of low temperature and light limitation on coccolithophores**
455 Our findings demonstrate that three coccolithophore strains maintain calcification
456 capabilities even under the low–temperature and light–limited conditions of the deep
457 sea (Figure 2). This persistence suggests that significant carbon export may occur much
458 deeper in the water column than previously recognized (Malinverno et al., 2003). Such
459 deep–sea calcification exerts distinct geochemical influences on the marine carbonate
460 system compared to surface processes, necessitating a comprehensive re–evaluation of
461 its impacts (Rigual–Hernández et al., 2020). Indeed, overlooking the contribution of
462 deep–dwelling coccolithophores may lead to a substantial underestimation of global
463 marine carbonate production (Rigual–Hernández et al., 2018). Beyond biogeochemistry,
464 investigating the resilience of these organisms under such stressors enhances our
465 understanding of the physiological limits of photosynthesis and provides critical
466 insights into life's adaptive strategies in extreme environments (Balch et al., 2023;
467 Chauhan et al., 2024). In conclusion, the adaptation of coccolithophores to the cold,
468 dark deep ocean reveals that fundamental biological forces driving global ecosystems
469 persist even in these seemingly barren reaches (Perrin et al., 2016).
470
471
472

References

Balch, W. M., Drapeau, D. T., Poulton, N., Archer, S. D., Cartisano, C., Burnell, C., and Godrijan, J.: Osmotrophy of dissolved organic compounds by coccolithophore populations: Fixation into particulate organic and inorganic carbon, Sci. Adv., 9, eadf6973, doi: 10.1126/sciadv.adf6973, 2023.

Beaufort, L., Couapel, M., Buchet, N., and Claustre, H.: Calcite production by coccolithophores in the South East Pacific Ocean: from desert to jungle, Biogeosciences Discuss., 4, 3267–3299, doi: 10.5194/bgd-4-3267-2007, 2007.

Borchard, C., Borges, A. V., Händel, N., and Engel, A.: Biogeochemical response of *Emiliania huxleyi* (PML B92/11) to elevated CO_2 and temperature under phosphorus limitation: A chemostat study, J. Exp. Mar. Biol. Ecol., 410, 61–71, https://doi.org/10.1016/j.jembe.2011.10.004, 2011.

Buitenhuis, E. T., Pangerc, T., Franklin, D. J., Le Quéré, C., and Malin, G.: Growth rates of six coccolithophorid strains as a function of temperature, Limnol. Oceanogr. 53, 1181–1185, doi:10.4319/lo.2008.53.3.1181, 2008.

Chauhan, N., Barton, S., Zarkogiannis, S., and Rickaby, R. E. M.: Light quality induces a shift in coccosphere morphology in *Scyphosphaera apsteinii*, J. Plankton. Res., 46, 383–386, doi: 10.1093/plankt/fbae032, 2024.

Conte, M. H., Sicre, M. A., Rühlemann, C., Weber, J. C., Schulte, S., Schulz–Bull, D., and Blanz, T.: Global temperature calibration of the alkenone unsaturation index (U_{37}^{K}) in surface waters and comparison with surface sediments, Geochem., Geophy., Geosys., 7, Q02005, doi: 10.1029/2005GC001054, 2006.

Conte, M. H., Thompson, A., Lesley, D., and Harris, R. P: Genetic and physiological influences on the alkenone/alkenoate versus growth temperature relationship in *Emiliania huxleyi* and *Gephyrocapsa oceanica*, Geochim. Cosmochim. Ac., 62,

51–68, doi: 10.1016/S0016-7037(97)00327-X, 1998.

Dedman, C. J., Barton, S., Fournier, M., and Richaby, R. E. M.: The cellular response to ocean warming in *Emiliania huxleyi*, Front. Microbiol., 14, 1177349, doi: 10.3389/fmicb.2023.1177349, 2023.

Dyhrman, S. T.: Nutrients and their acquisition: phosphorus physiology in microalgae, in: The physiology of microalgae, edited by: Borowitzka, M. A., Beardall, J., and Raven, J. A., Springer, Heidelberg, Germany, 155–183, https://doi.org/10.1007/978-3-319-24945-2, 2016.

Fabry, V. J., and Balch, W. M.: Direct measurements of calcification rates in planktonic organisms, in: Guide to best practices for ocean acidification research and data reporting, edited by Riebesell, U., Fabry, V. J., Hansson, L., and Gattuso, J. P., Luxembourg, Publications Office of the European Union, 201–212, https://doi.org/10.2777/66906, 2010.

Feng, Y., Warner, M. E., Zhang, Y., Sun, J., Fu, F., Rose, J. M., and Hutchins, D. A.: Interactive effects of increased pCO_2, temperature and irradiance on the marine coccolithophore *Emiliania huxleyi* (Prymnesiophyceae), Eur. J. Phycol., 43, 87–98, https://doi.org/10.1080/09670260701664674, 2008.

Gafar, N. A., Eyre, B. D., and Schulz, K. G.: A conceptual model for projecting coccolithophorid growth, calcification and photosynthetic carbon fixation rates in response to global ocean change, Front. Mar. Sci., 4, 433, doi: 10.3389/fmars.2017.00433, 2018.

Gerecht, A. C., Šupraha, L., Edvardsen, B., Probert, I., and Henderiks, J.: High temperature decreases the PIC / POC ratio and increases phosphorus requirements in *Coccolithus pelagicus* (Haptophyta), 11, 3531–3545, doi: 10.5194/bg-11-3531-2014, 2014.

Guillard, R. R. L., and Ryther, J. H.: Studies of marine planktonic diatoms. I. Cyclotella nana Hustedt and Detonula confervacea Cleve. Can. J. Microbiol., 8, 229–239, doi:10. 1139/m62-029, 1962.

Hernández–Almeida, I., Krumhardt K. M., Zhang H., and Stoll H. M.: Estimation of physiological factors controlling carbon isotope fractionation in coccolithophores in photic zone and core–top samples, Geochem. Geophy. Geosy., 21, e2020GC009272, doi: 10.1029/2020GC009272, 2020.

Horváth, G., and Varjú, D.: Polarized light in animal vision: polarization patterns in nature, Springer, Berlin, 319–324, https:doi//10.1007/978-3-662-09387-0, 2004.

Jin, P., Liu, N., and Gao, K.: Physiological responses of a coccolithophore to multiple environmental drivers, Mar. Pollut. Bull., 146, 225–235, doi:10.1016/j.marpolbul.2019.06.032, 2019.

Jordan, R. W., and Winter, A.: Assemblages of coccolithophorids and other living microplankton off the coast of Puerto Rico during January–May 1995, Mar. Micropaleontol., 39, 113–130, dio: 10.1016/S0377-8398(00)00017-7, 2000.

Li, S., Zhu, J., Jin, X., Feng, Y., Jiao, N., and Zhang, W.: Multifaceted contributions of coccolithophores to ocean carbon export, Ocean-Land-Atmos. Res., 3, Article0049, doi: 10.34133/olar.0049, 2024.

Malinverno, E., Ziveri, P., and Corselli, C.: Coccolithophorid distribution in the Ionian Sea and its relationship to eastern Mediterranean circulation during late fall to early winter 1997, J. Geophys. Res., 108(C9), 8115, doi: 10.1029/2002JC001346, 2003.

Masuko, T., Minami, A., Iwasaki, N., Majima, T., Nishimura, S. I., and Lee, Y. C.: Carbohydrate analysis by a phenolsulfuric acid method in microplate format, Anal. Biochem., 339, 69–72. doi:10.1016/j.ab.2004.12.001, 2005.

548 McKew, B. A., Lefebvre, S. C., Achterberg, E. P., Metodieva, G., Raines, C. A.,
549 Metodiev, M. V., and Geider, R. J.: Plasticity in the proteome of *Emiliania huxleyi*
550 CCMP 1516 to extremes of light is highly targeted, New Phytol., 200, 61–73, doi:
551 10.1111/nph.12352, 2013.
552 Pakulski, J. D., and Benner, R: An improved method for the hydrolysis and MBTH
553 analysis of dissolved and particulate carbohydrates in seawater, Mar. Chem., 40,
554 143–160, doi:10.1016/0304-4203(92)90020-B, 1992.
555 Perrin, L., Probert, I., Langer, G., and Aloisi, G.: Growth of the coccolithophore
556 *Emiliania huxleyi* in light– and nutrient–limited batch reactors: relevance for the
557 BIOSOPE deep ecological niche of coccolithophores, Biogeosciences, 13, 5983–
558 6001, doi: 10.5194/bg-13-5983-2016, 2016.
559 Petrou, K., Kranz, S. A., Trimborn, S., Hassler, C. S., Ameijeiras, S. B., Sackett, O.,
560 Ralph, P. J., and Davidson, A. T.: Southern Ocean phytoplankton physiology in a
561 changing climate, J. Plant Physiol., 203, 135–150, doi:
562 10.1016/j.jplph.2016.05.004, 2016.
563 Pierangelini, M., Stojkovic, S., Orr, P. T., and Beardall J.: Photo-acclimation to low
564 light–Changes from growth to antenna size in the cyanobacterium
565 *Cylindrospermopsis raciborskii*, Harmful Algae, 46, 11–17, doi:
566 10.1016/j.hal.2015.04.004, 2015.
567 Potts, M., and Friedmann, E.: Effects of water stress on cryptoendolithic cyanobacteria
568 from hot desert rocks, Arch Microbiol., 130, 267–271, doi: 10.1007/BF00425938,
569 1981.
570 Poulton, A. J., Stinchcombe, M. C., Achterberg, E. P., Bakker, D. C. E., Dumousseaud,
571 C., Lawson, H. E., Lee, G. A., Richier, S., Suggett, D. J., and Young, J. R.:
572 Coccolithophores on the north–west European shelf: calcification rates and

environmental controls, Biogeosciences, 11, 3919–3940, doi: 10.5194/bg-11-3919-2014, 2014.

R Core Team: The R foundation for statistical computing platform, x86_64-w64-mingw32/x64, available at: https://cran.r-project.org/bin/windows/base/old/3.5.0/ (28 February 2020), 2018.

Rigual–Hernández, A. S., Trull, T. W., Nodder, S. D., Flores, J. A., Bostock, H., Abrantes, F., Eriksen, R. S., Sierro, F. J., Davies, D. M., Ballegeer, A. M., Fuertes, M. A., and Northcote, L. C.: Coccolithophore biodiversity controls carbonate export in the Southern Ocean, Biogeosciences, 17, 245–263, 2020.

Rigual–Hernández, A., Flores, J. A., Sierro, F. J., Fuertes, M. A., Cros, L., and Trull, T. W.: Coccolithophore populations and their contribution to carbonate export during an annual cycle in the Australian section of the Antarctic zone, Biogeosciences, 15, 1843–1862, doi: 10.5194/bg-15-1843-2018, 2018.

Ritchie, R. J.: Consistent sets of spectrophotometric chlorophyll equations for acetone, methanol and ethanol solvents, Photosynth Res., 89, 27–41, doi: 10.1007/s11120-006-9065-9, 2006.

Rosas–Navarro, A., Langer, G., and Ziveri, P.: Temperature affects the morphology and calcification of *Emiliania huxleyi* strains, Biogeosciences, 13, 2913–2926, doi: 10.5194/bg-13-2913-2016, 2016.

Sage, R. F.: Variation in the kcat of Rubisco in C3 and C4 plants and some implications for photosynthetic performance at high and low temperature, J. Experimental Botany, 53: 609–620, doi: 10.1016/j.jplph.2016.05.004, 2016.

Shen, L., Ren, F., Wang, Y. C., Li, Z., Zheng, M., Li, X., Fan, W., Yang, Y., Sang, M., Liu, C. Han, G., Qin, S., Fan, J., Tian, L., Kuang, T., Shen, J. R., and Wang, W.: Structure and function of a huge photosystem I-fucoxanthin chlorophyll

598 supercomplex from a coccolithophore, Science, 389, eadv2132, doi:
599 10.1126/science.adv2132, 2025a.
600 Shen, Y., Jiang, R., Chang, J., Cai, L., Zhu, Y., Yin, Y., Shao, L., Wu, M., Zhang, J., and
601 He, P.: The effect of temperature on the photosynthetic carbon fixation efficiency
602 of sessile macroalgae in the mussel farming area of Guoqi Island through stable
603 isotope, Mar. Environ. Res., 209, 107190, doi: 10.1016/j.marenvres.2025.107190,
604 2025b.
605 Sheward, R. M., Liefer, J. D., Irwin, A. J., and Finkel, Z. V.: Elemental stoichiometry
606 of the key calcifying marine phytoplankton *Emiliania huxleyi* under ocean climate
607 change: A meta–analysis, Glob. Change Biol., 29, 4259–4278,
608 doi:10.1111/gcb.16807, 2023.
609 Skeffington, A., Fischer, A., Sviben, S., Brzezinka, M., Górka, M., Bertinetti, L.,
610 Woehle, C., Huettel, B., Graf, A., and Scheffel, A.: A joint proteomic and genomic
611 investigation provides insights into the mechanism of calcification in
612 coccolithophores, Nature Commun., 24, 3749, doi: 10.1038/s41467-023-39336-1
613 Solorzano, L., and Sharp, J. H.: Determination of total dissolved phosphorus and
614 particulate phosphorus in nature waters, Limnol. Oceanogr., 25, 754–758,
615 doi:10.4319/lo.1980.25.4.0754, 1980.
616 Strzepek, R. F., Boyd, P. W., and Sunda, W. G.: Photosynthetic adaptation to low iron,
617 light, and temperature in Southern Ocean phytoplankton, Proc. Nat. Acad. Sci. U.
618 S., 116, 4388–4393, doi: 10.1073/pnas.1810886116, 2019.
619 Sui, Y., Muys, M., Van de Waal, D. B., D'Adamo, S., Vermeir, P., Fernandes, T. V., and
620 Vlaeminck, S. E.: Enhancement of co–production of nutritional protein and
621 carotenoids in *Dunaliella salina* using a two–phase cultivation assisted by nitrogen
622 level and light intensity, Bioresour. Technol., 287, 121398,

http://doi.org/10.1016/j.biortech.2019.121398, 2019.

Tong, S., Hutchins, D. A., and Gao, K.: Physiological and biochemical responses of *Emiliania huxleyi* to ocean acidification and warming are modulated by UV radiation, Biogeosciences, 16, 561–572, https://doi.org/10.5194/bg-16-561-2019, 2019.

Torres–Romero, I., Clark, A. J., Wijker, R. S., Jaggi, M., Zhang, H., and Stoll, H. M.: Temperature–dependent carbon isotope fractionation in coccolithophores, Front. Earth Sci., 12, 1331179, doi: 10.3389/feart.2024.1331179, 2024.

Triccas, A., Chevrier, D. M., Verezhak, M., Ihli, J., Guizar-Sicairos, M., Holler, M., Scheffel, A., Ozaki, N., Chamard, V., Wood, R., Grünewald, T. A., and Nudelman, F.: Dynamic change of calcium-rich compartments during coccolithophore biomineralization, Sci. Adv., 11, eadv0618, doi: 10.1126/sciadv.adv0618, 2025.

Wang, D., Gao, X., Wang, X., Yuan, X., Guo, X., Zhang, Y., Xu, K., and Li, Z.: Diverse thermal responses of the growth, photosynthesis, lipid and fatty acids in the terrestrial oil–producing microalga *Vischeria* sp. WL1, J. Appl. Phycol., 36, 29–39, doi:10.1007/s10811-023-03152-3, 2024.

Wang, X., Fu, F., Qu, P., Kling, J. D., Jiang, H., Gao, Y., and Hutchins, D. A.: How will the key marine calcifier *Emiliania huxleyi* respond to a warmer and more thermally variable ocean? Biogeosciences, 16, 4393–4409, doi: 10.5194/bg-16-4393-2019, 2019.

Xu, J., Li, T., Li, C. L., Zhu, S. N., Wang, Z. M., and Zeng, E. Y.: Lipid accumulation and eicosapentaenoic acid distribution in response to nitrogen limitation in microalga *Eustigmatos vischeri* JHsu-01 (Eustigmatophyceae), Algal Res., 48, 101910, doi: 10.1016/j.algal.2020,101910, 2020.

Young, J. N., Goldman, J. A. L., Kranz, S. A., Tortell, P. D., and Morel, F. M. M.: Slow

carboxylation of Rubisco constrains the rate of carbon fixation during Antarctic phytoplankton blooms, New Phytol., 205, 172–181, doi: 10.1111/nph.13021, 2015.

Young, J. R., Davis, S. A., Bown, P. R., and Mann, S.: Coccolith ultrastructure and biomineralisation, J. Struct. Biol., 126, 195–215, doi: 10.1006/jsbi.1999.4132, 1999.

Zhang, Y., and Gao, K.: Photosynthesis and calcification of the coccolithophore *Emiliania huxleyi* are more sensitive to changed levels of light and CO_2 under nutrient limitation, J. Photochem. Photobiol. B: Biol., 217, 112145, doi: 10.1016/j.jphotobiol.2021.112145, 2021.

Zhang, Y., Bach, L. T., Schulz, K. G., and Riebesell, U.: The modulating effect of light intensity on the response of the coccolithophore *Gephyrocapsa oceanica* to ocean acidification, Limnol. Oceanogr., 60, 2145–2157, doi: 10.1002/lno.10161, 2015.

Zhang, Y., Collins, S., and Gao, K.: Reduced growth with increased quotas of particulate organic and inorganic carbon in the coccolithophore *Emiliania huxleyi* under future ocean climate change conditions, Biogeosciences, 17, 6357–6375, doi:10.5194/bg-17-6357-2020, 2020.

Zhang, Y., Li, Z., Schulz, K. G., Hu, Y., Irwin, A. J., and Finkel, Z. V.: Growth-dependent changes in elemental stoichiometry and macromolecular allocation in the coccolithophore *Emiliania huxleyi* under different environmental conditions, Limnol. Oceanogr., 66, 2999–3009, doi: 10.1002/lno.11854, 2021.

Zweifel, S. T., Henshaw, R. J., Müller, O., Keegstra, J. M., Charlton, S. G. V., Pioli, R., Martínez-Pérez, C., Alcolombri, U., Clerc, E., and Stocker, R.: Bacteria induce an amoeboid phase in coccolithophores that persists after bloom collapse, Sci. Adv., 11, eadw7280, http://doi.org/10.1126/sciadv.adw7280, 2025.

Data availability. The data are available upon request to the corresponding author (Yong Zhang)

Author contributions. YZ and JS designed the experiment. YW performed the experiment. WK and JS analyzed the data and wrote the first manuscript. All authors improved and reviewed the manuscript. JS, WK and YW contributed equally to this work.

Competing interests. The authors declare that they have no conflict of interest.

Financial support. This study was supported by the National Natural Science Foundation of China (No. 32270397), Natural Science Foundation of Xinjiang Uygur Autonomous Region (No. 202501A54), the Xinjiang Normal University Landmark Achievements Cultivation Project (XJNUZBS2401), the Tianchi Talent Program in Xinjiang Uyghur Autonomous Region, and by Hubei Provincial Department of Education Scientific Research Plan Guidance Project (B2019435), China; Natural Science Foundation of Fujian Province (2023J01290), China; and the "GeoX" Interdisciplinary, Research Funds for the Frontiers Science Center for Critical Earth Material Cycling, Nanjing University (020614380194), China.

Figure Legends

Figure 1. Under the treatments of low temperature (LT, 9 ºC) and low light (LL, 15 μmol photons m^{-2} s^{-1}), LTHL (9 ºC, 150 μmol photons m^{-2} s^{-1}), HTLL (21 ºC, 15 μmol photons m^{-2} s^{-1}) and HTHL (21 ºC, 150 μmol photons m^{-2} s^{-1}), growth rates and cellular contents of chlorophyll *a* of *Gephyrocapsa oceanica* NIES–1318, *Emiliania huxleyi* PML B92/11 and *E. huxleyi* RCC1266. Data are presented as mean ± standard deviation for three replicates (n = 3). Different letters (a, b, c, d) represent significant differences between treatments (Tukey, $p < 0.05$).

Figure 2. Under the treatments of low temperature (LT, 9 ºC) and low light (LL, 15 μmol photons m^{-2} s^{-1}), LTHL (9 ºC, 150 μmol photons m^{-2} s^{-1}), HTLL (21 ºC, 15 μmol photons m^{-2} s^{-1}) and HTHL (21 ºC, 150 μmol photons m^{-2} s^{-1}), cellular contents of particulate inorganic carbon (PIC), particulate organic carbon (POC), particulate organic nitrogen (PON), particulate organic phosphorus (POP) of *Gephyrocapsa oceanica* NIES–1318, *Emiliania huxleyi* PML B92/11 and *E. huxleyi* RCC1266. Data are presented as mean ± standard deviation for three replicates (n = 3). Different letters (a, b, c, d) represent significant differences between treatments (Tukey, $p < 0.05$).

Figure 3. Under the treatments of low temperature (LT, 9 ºC) and low light (LL, 15 μmol photons m^{-2} s^{-1}), LTHL (9 ºC, 150 μmol photons m^{-2} s^{-1}), HTLL (21 ºC, 15 μmol photons m^{-2} s^{-1}) and HTHL (21 ºC, 150 μmol photons m^{-2} s^{-1}), the ratios of PIC : POC, POC : PON, POC : POP, PON : POP of *Gephyrocapsa oceanica* NIES–1318, *Emiliania huxleyi* PML B92/11 and *E. huxleyi* RCC1266. Data are presented as mean ± standard deviation for three replicates (n = 3). Different letters (a, b, c) represent significant differences between treatments (Tukey, $p < 0.05$).

Figure 4. Under the treatments of low temperature (LT, 9 ºC) and low light (LL, 15 μmol photons m^{-2} s^{-1}), LTHL (9 ºC, 150 μmol photons m^{-2} s^{-1}), HTLL (21 ºC, 15 μmol photons m^{-2} s^{-1}) and HTHL (21 ºC, 150 μmol photons m^{-2} s^{-1}), cellular contents of carbohydrate and lipid of *Gephyrocapsa oceanica* NIES–1318, *Emiliania huxleyi* PML B92/11 and *E. huxleyi* RCC1266. Data are presented as mean ± standard deviation for three replicates (n = 3). Different letters (a, b, c) represent significant differences between treatments (Tukey, $p < 0.05$).

Figure S1. Under the treatments of low temperature (LT, 9 ºC) and low light (LL, 15 μmol photons m^{-2} s^{-1}), LTHL (9 ºC, 150 μmol photons m^{-2} s^{-1}), HTLL (21 ºC, 15 μmol photons m^{-2} s^{-1}) and HTHL (21 ºC, 150 μmol photons m^{-2} s^{-1}), growth curves of *Gephyrocapsa oceanica* NIES–1318, *Emiliania huxleyi* PML B92/11 and *E. huxleyi* RCC1266. Data are presented as mean ± standard deviation for three replicates (n = 3).

Figure S2. Under the treatments of low temperature (LT, 9 ºC) and low light (LL, 15 μmol photons m^{-2} s^{-1}), LTHL (9 ºC, 150 μmol photons m^{-2} s^{-1}), HTLL (21 ºC, 15 μmol photons m^{-2} s^{-1}) and HTHL (21 ºC, 150 μmol photons m^{-2} s^{-1}), the ratios of carbohydrate : POC and lipid : POC of *Gephyrocapsa oceanica* NIES–1318, *Emiliania huxleyi* PML B92/11 and *E. huxleyi* RCC1266. Data are presented as mean ± standard deviation for three replicates (n = 3). Different letters (a, b, c) represent significant differences between treatments (Tukey, $p < 0.05$).

748 **Table 1.** Temperature (9 and 15 ºC), light intensity (*, 15 and 150 μmol photons m^{-2} s^{-1}), growth rate (μ in d^{-1}), and cellular contents (pg $cell^{-1}$) of chlorophyll (Chl) *a*, PIC, POC, PON and POP, the ratios of PIC : POC, POC : PON, POC : POP, and PON : POP, as well as carbohydrate (Carbo) and lipid contents (pg $cell^{-1}$). The values are expressed as the mean ± standard deviations in the brackets of three replicates.

		G. oceanica NIES–1318		*E. huxleyi* PML B92/11		*E. huxleyi* RCC1266	
		15*	150	15	150	15	150
μ	9ºC	0.24(0.04)	0.67(0.01)	0.46(0.04)	0.60(0.01)	0.45(0.03)	0.65(0.02)
	21ºC	0.85(0.03)	1.29(0.01)	0.79(0.01)	1.26(0.02)	0.84(0.04)	1.25(0.01)
Chl *a*	9ºC	0.30(0.04)	0.25(0.01)	0.25(0.02)	0.23(0.02)	0.30(0.07)	0.24(0.03)
	21ºC	0.34(0.05)	0.33(0.01)	0.39(0.02)	0.27(0.03)	0.32(0.06)	0.30(0.03)
PIC	9ºC	4.29(0.51)	2.69(0.38)	4.38(1.19)	3.39(1.01)	4.10(1.11)	1.99(0.66)
	21ºC	4.94(0.25)	8.01(0.40)	7.01(2.09)	9.82(0.37)	10.91(1.53)	14.18(1.35)
POC	9ºC	10.41(0.68)	12.01(1.09)	10.32(0.78)	11.78(0.86)	9.67(0.97)	11.78(0.78)
	21ºC	22.64(2.27)	31.74(1.32)	21.21(1.49)	34.63(1.62)	21.45(3.10)	31.31(1.59)
PON	9ºC	4.71(0.62)	3.60(0.05)	3.09(0.29)	2.40(0.32)	3.40(0.85)	2.26(0.12)
	21ºC	5.65(0.80)	6.21(0.30)	4.55(0.11)	5.60(0.15)	4.17(0.44)	5.14(0.51)
POP	9ºC	0.39(0.11)	0.46(0.04)	0.38(0.03)	0.45(0.04)	0.38(0.07)	0.39(0.01)
	21ºC	0.51(0.08)	0.53(0.03)	0.50(0.05)	0.54(0.06)	0.45(0.06)	0.50(0.02)
PIC:POC	9ºC	0.41(0.05)	0.23(0.03)	0.42(0.10)	0.29(0.08)	0.42(0.08)	0.17(0.05)
	21ºC	0.22(0.02)	0.25(0.02)	0.33(0.10)	0.28(0.02)	0.51(0.05)	0.46(0.06)
POC:PON	9ºC	2.60(0.21)	3.89(0.36)	3.94(0.66)	5.75(0.33)	3.45(0.83)	6.09(0.54)
	21ºC	4.74(0.84)	5.97(0.42)	5.45(0.51)	7.23(0.52)	5.98(0.32)	7.13(0.42)
POC:POP	9ºC	72.1(18.7)	67.9(3.2)	71.1(10.3)	68.0(3.0)	65.8(6.5)	77.9(5.0)
	21ºC	116.9(23.4)	154.6(1.5)	111.3(16.8)	165.5(12.7)	122.5(5.7)	163.3(14.1)
PON:POP	9ºC	27.80(6.76)	17.54(1.67)	18.09(0.39)	11.86(0.67)	19.81(5.09)	12.82(0.66)
	21ºC	24.62(0.52)	25.98(2.05)	20.36(1.58)	23.05(3.16)	20.49(0.58)	22.99(2.83)
Carbo	9ºC	0.37(0.03)	3.01(0.07)	0.41(0.08)	2.65(0.14)	0.38(0.06)	2.98(0.05)
	21ºC	0.98(0.05)	5.66(0.16)	1.10(0.37)	5.43(0.58)	0.97(0.15)	5.18(0.21)
Lipid	9ºC	1.38(0.24)	8.07(0.33)	1.03(0.11)	4.36(0.79)	0.87(0.09)	6.42(2.02)
	21ºC	4.17(0.21)	13.37(0.62)	4.23(0.20)	12.12(0.57)	4.69(0.36)	12.82(0.39)

753

754

755

756

757

758

759

760

761

762

763 **Table 2.** Results of two–way ANOVAs of the impacts of temperature (T), light intensity
764 (L) and their interaction (T×L) on growth rate (μ), chlorophyll (Chl) *a*, PIC, POC, PON
765 and POP contents, PIC : POC ratio, POC : PON ratio, POC : POP ratio, PON : POP
766 ratio, as well as carbohydrate (Carbo) and lipid contents.

		G. oceanica NIES–1318		*E. huxleyi* PML B92/11		*E. huxleyi* RCC1266	
	Factor	*F* value	*p* value	*F* value	*p* value	*F* value	*p* value
μ	T	1950.0	<0.001	1362.4	<0.001	1006.3	<0.001
	L	991.0	<0.001	518.8	<0.001	384.8	<0.001
	T×L	0.16	=0.702	161.5	<0.001	45.60	<0.001
Chl *a*	T	11.9	=0.009	66.6	<0.001	3.6	=0.094
	L	2.9	=0.128	39.4	<0.001	1.5	=0.261
	T×L	1.5	=0.254	18.3	=0.003	0.2	=0.669
PIC	T	168.6	<0.001	35.6	<0.001	185.2	<0.001
	L	10.2	=0.013	1.4	=0.267	0.7	=0.427
	T×L	103.2	<0.001	6.3	=0.037	14.9	=0.005
POC	T	358.7	<0.001	552.6	<0.001	215.3	<0.001
	L	40.2	<0.001	107.4	<0.001	31.4	<0.001
	T×L	19.8	=0.002	69.4	<0.001	13.2	=0.007
PON	T	34.1	<0.001	289.8	<0.001	33.9	<0.001
	L	0.8	=0.397	1.8	=0.221	0.1	0.793
	T×L	7.5	=0.025	40.2	<0.001	11.3	=0.010
POP	T	5.4	=0.049	15.1	=0.005	9.6	=0.015
	L	1.1	=0.324	4.4	=0.068	0.8	=0.394
	T×L	0.3	=0.618	0.2	=0.673	0.5	=0.516
PIC : POC	T	19.5	=0.002	0.9	=0.360	26.9	=0.001
	L	17.2	=0.003	3.8	=0.086	17.8	=0.003
	T×L	35.4	<0.001	0.9	=0.379	7.3	=0.027
POC : PON	T	50.5	<0.001	25.2	=0.001	30.6	=0.001
	L	18.2	=0.003	36.1	<0.001	34.4	<0.001
	T×L	0.1	=0.917	0.1	=0.961	5.3	=0.050
POC : POP	T	57.0	<0.001	101.8	<0.001	203.7	<0.001
	L	3.7	=0.090	14.1	=0.006	28.2	=0.001
	T×L	5.8	=0.043	17.6	=0.003	8.3	=0.020
PON : POP	T	1.6	=0.245	41.5	<0.001	10.2	=0.013
	L	4.5	=0.067	2.9	=0.128	1.7	=0.223
	T×L	7.6	=0.024	18.3	=0.003	7.8	=0.023
Carbo	T	941.5	<0.001	73.1	<0.001	316.3	<0.001
	L	4773.8	<0.001	262.8	<0.001	1896.6	<0.001
	T×L	370.3	<0.001	26.5	=0.001	105.7	<0.001
Lipid	T	333.3	<0.001	359.6	<0.001	71.7	<0.001

	L	1281.1	<0.001	377.7	<0.001	128.6	<0.001
	T×L	32.1	<0.001	62.3	<0.001	4.6	=0.065

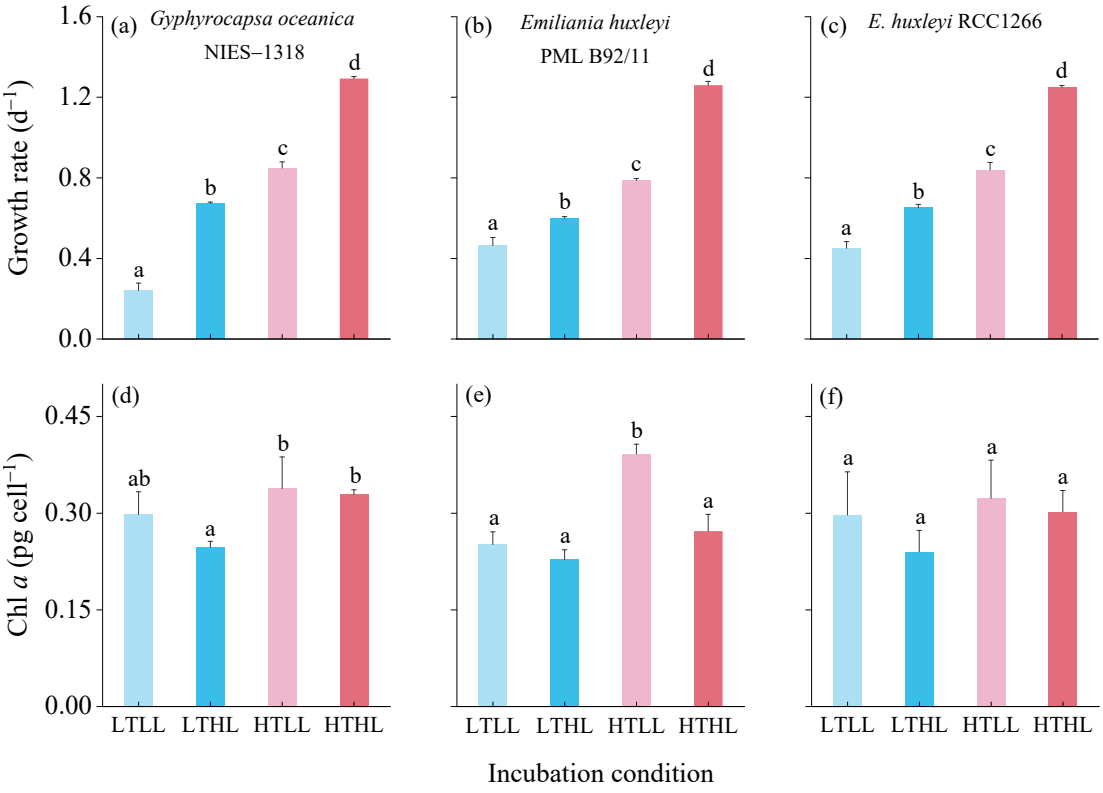
(a) Gyphyrocapsa oceanica
NIES–1318
(b) Emiliania huxleyi
PML B92/11
(c) E. huxleyi RCC1266
Growth rate (d⁻¹)
Chl a (pg cell⁻¹)
(d)
(e)
(f)
LTLL
LTHL
HTLL
HTHL
Incubation condition

Figure 1

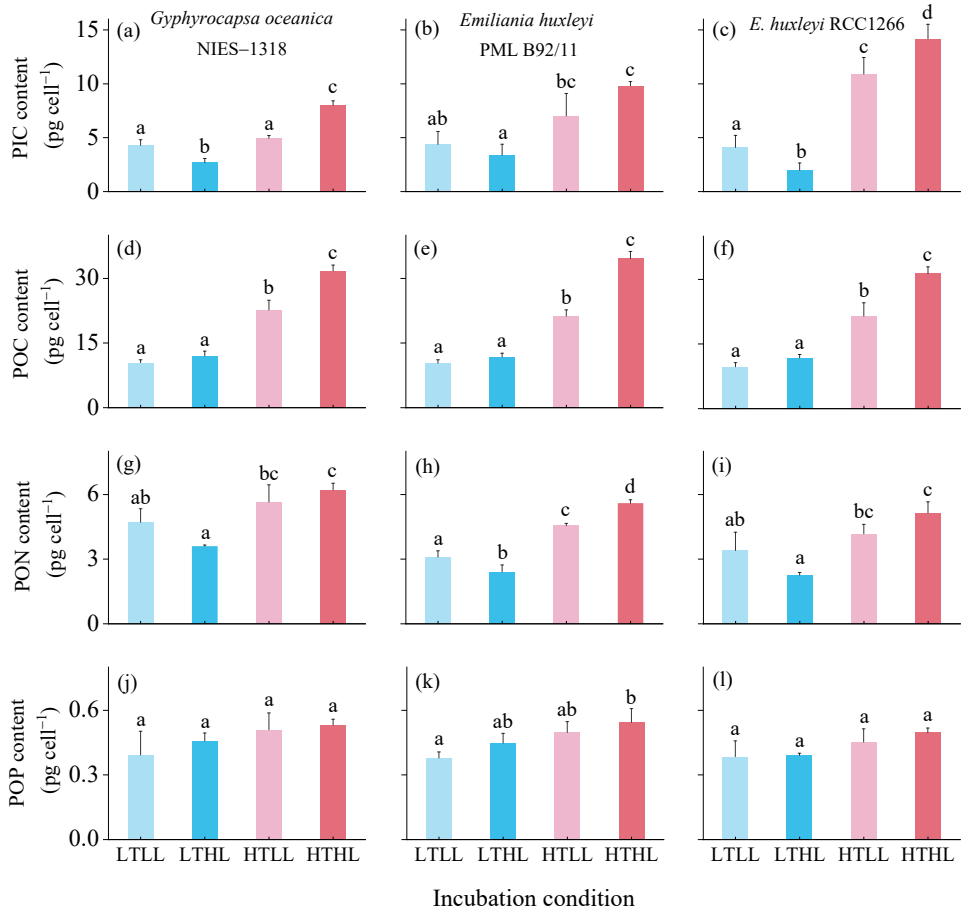
(a) Gyphyrocapsa oceanica NIES–1318
(b) Emiliania huxleyi PML B92/11
(c) E. huxleyi RCC1266
PIC content (pg cell⁻¹)
POC content (pg cell⁻¹)
PON content (pg cell⁻¹)
POP content (pg cell⁻¹)
LTLL LTHL HTLL HTHL
Incubation condition

Figure 2

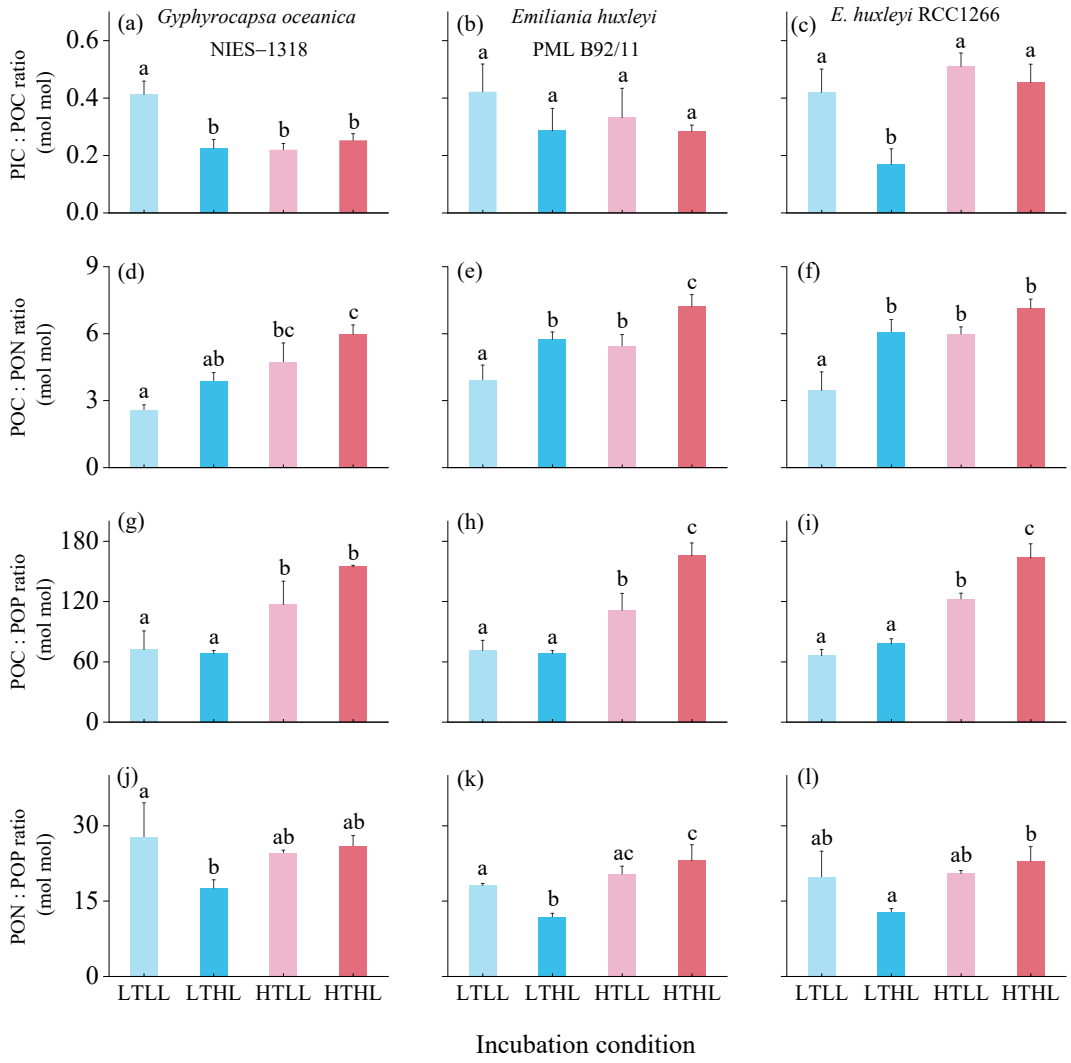
(a) Gyphyrocapsa oceanica NIES–1318
(b) Emiliania huxleyi PML B92/11
(c) E. huxleyi RCC1266
PIC : POC ratio (mol mol)
POC : PON ratio (mol mol)
POC : POP ratio (mol mol)
PON : POP ratio (mol mol)
LTLL LTHL HTLL HTHL
Incubation condition

Figure 3

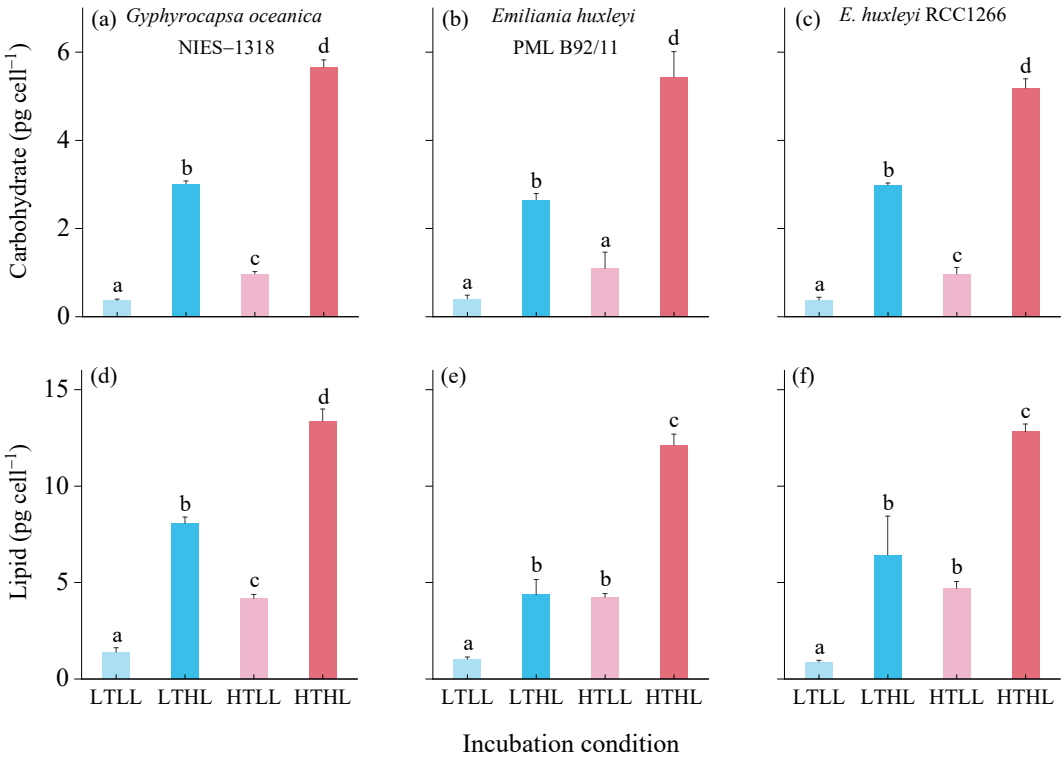
(a) Gyphyrocapsa oceanica
NIES−1318
(b) Emiliania huxleyi
PML B92/11
(c) E. huxleyi RCC1266
Carbohydrate (pg cell−1)
Lipid (pg cell−1)
(d)
(e)
(f)
LTLL
LTHL
HTLL
HTHL
Incubation condition

Figure 4

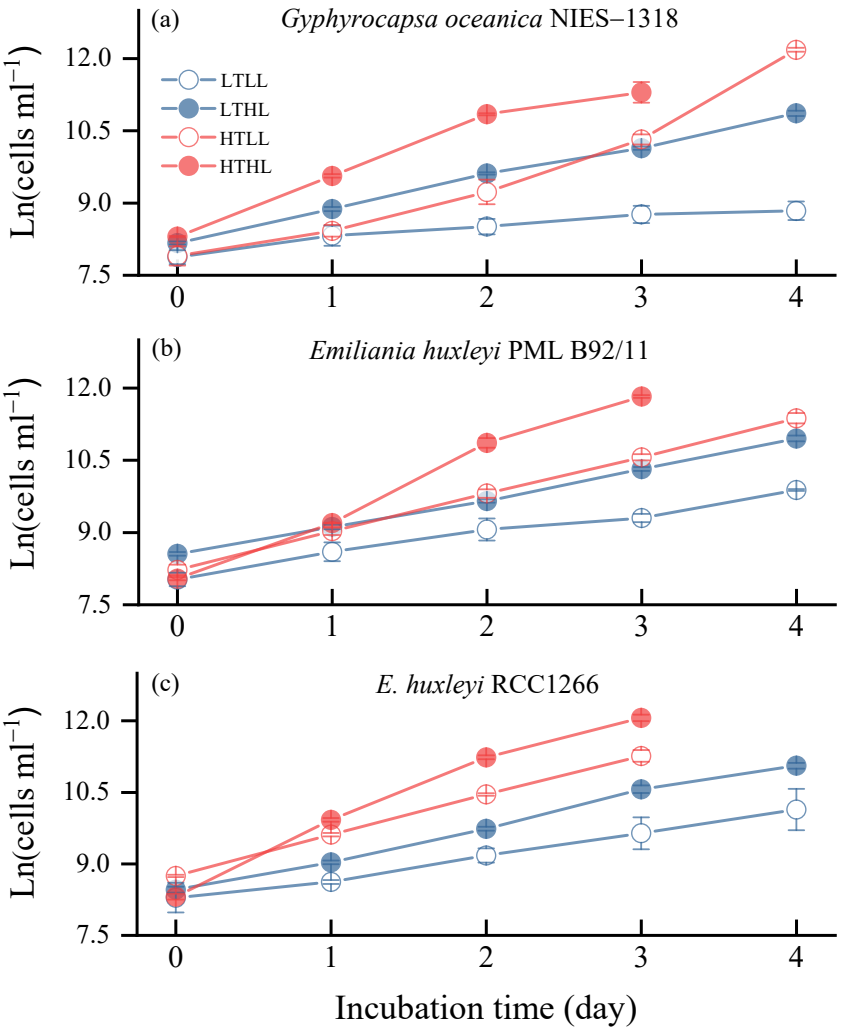
(a)
Gyphyrocapsa oceanica NIES−1318
LTLL
LTHL
HTLL
HTHL
(b)
Emiliania huxleyi PML B92/11
(c)
E. huxleyi RCC1266
Ln(cells ml−1)
12.0
10.5
9.0
7.5
0
1
2
3
4
Incubation time (day)

Figure S1

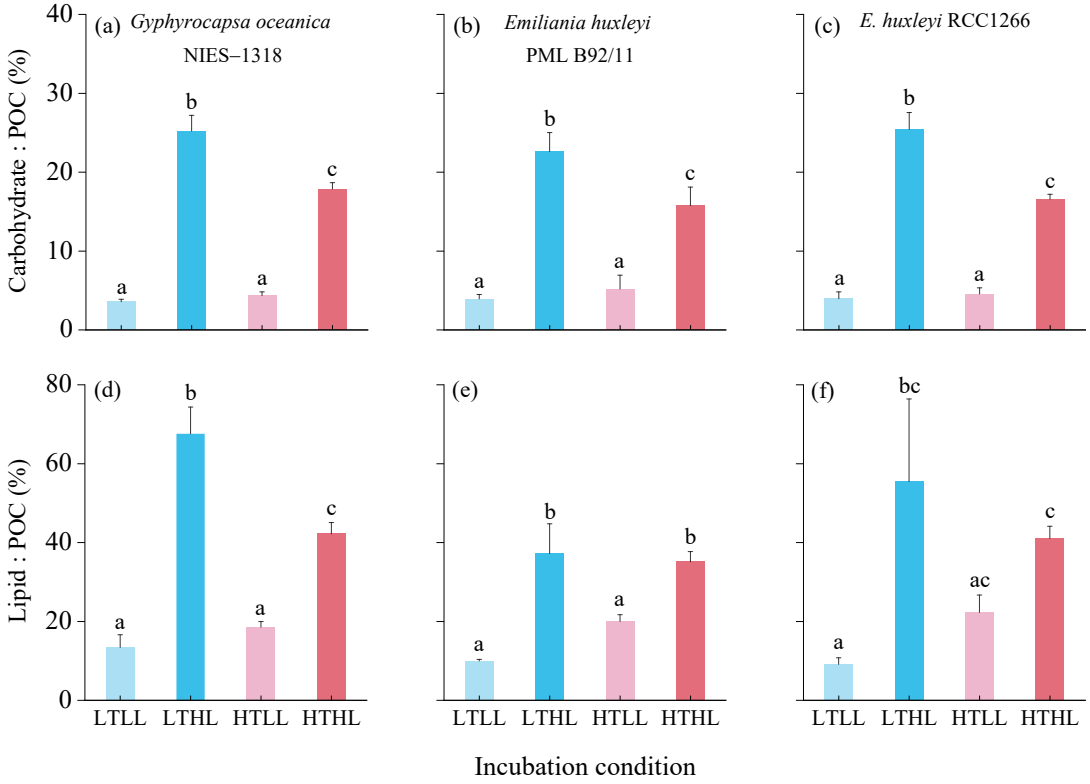
(a) Gyphyrocapsa oceanica
NIES−1318
(b) Emiliania huxleyi
PML B92/11
(c) E. huxleyi RCC1266
Carbohydrate : POC (%)
Lipid : POC (%)
(d)
(e)
(f)
LTLL LTHL HTLL HTHL
Incubation condition

Figure S2